Ferromagnetism and Wigner crystallization in kagome graphene and related structures

Yuanping Chen,[1,*] Shenglong Xu,[2,3] Yuee Xie,[1] Chengyong Zhong,[1] Congjun Wu,[3] and S. B. Zhang[4]

[1]*Department of Physics, Xiangtan University, Xiangtan 411105, People's Republic of China*

[2]*Condensed Matter Theory Center and Joint Quantum Institute, Department of Physics, University of Maryland, College Park, Maryland 20742, USA*

[3]*Department of Physics, University of California, San Diego, California 92093, USA*

[4]*Department of Physics, Applied Physics, and Astronomy, Rensselaer Polytechnic Institute, Troy, New York 12180, USA*

(Received 8 April 2018; revised manuscript received 4 July 2018; published 23 July 2018)

Interaction in a flat band is magnified due to the divergence in the density of states, which gives rise to a variety of many-body phenomena such as ferromagnetism and Wigner crystallization. Until now, however, most studies of flat-band physics have been based on model systems, making their experimental realization something that would occur in the distant future. Here, we propose a class of systems made of real atoms, namely carbon atoms with realistic physical interactions (dubbed here "kagome graphene/graphyne"). Density functional theory calculations reveal that these kagome lattices offer a controllable way to realize robust flat bands sufficiently close to the Fermi level. Upon hole doping, they split into spin-polarized bands at different energies to result in a flat-band ferromagnetism. At half-filling, this splitting reaches its highest level of 768 meV. At smaller fillings, e.g., when $\nu = \frac{1}{6}$, on the other hand, a Wigner crystal spontaneously forms, where the electrons form closed loops localized on the grid points of a regular triangular lattice. It breaks the translational symmetry of the original kagome lattice. We further show that the kagome lattices exhibit good mechanical stabilities, based on which a possible route for experimental realization of the kagome graphene is also proposed.

DOI: 10.1103/PhysRevB.98.035135

I. INTRODUCTION

Carbon is one of the most abundant elements in the universe. To date, a large number of carbon allotropes have been found or synthesized, including fullerene, carbon nanotubes, and graphene [1–3]. Graphene is by far the most celebrated carbon material [4] due to its excellent properties, such as an extremely high carrier mobility [5,6] and thermal conductivity [7], and mechanical strength [8] with enormous potentials for applications [9–15]. On the other hand, the Coulomb interaction energy in graphene is small when compared with the kinetic energy. In a conventional view, this would imply that carbon is not a good candidate for studying the physics of strongly correlated systems. Furthermore, the strength of the spin-orbit coupling in carbon is exceptionally small [16], which constrains its usefulness in studying topological physics.

On the other hand, flat band systems are important for both strong interactions and topological physics. Here, regardless of its absolute value, interaction energy dominates over kinetic energy due to the quench of the latter. The interplay between a band flatness and interaction energy has given rise to a variety of strong correlation phenomena, such as a flat-band ferromagnetism [17,18] and Wigner crystallization [19] in the context of a kagome lattice [20] and the p_x-p_y-orbital bands of honeycomb [21–23] and Lieb lattices [24–26]. In these systems, due to a destructive interference among the hopping processes, the single-particle eigenstates become localized degenerate states at different plaquettes. The Bloch-wave band states are a superposition of these localized states, and hence they are dispersionless. Recently, Wigner crystallization has also been identified in nearly flat topological bands at low fillings [27]. The salient feature of the flat bands has prompted suggestions to use it to boost the superconducting transition temperature [28] and to host topological states such as fractional quantum Hall states. A combination of nontrivial topology and strong correlation may lead to exotic phenomena as a result of fractional excitations of anyons and fractional statistics. Recently, fractional Chern insulators based on the flat band structure have also been studied extensively in lattice systems in the absence of magnetic Landau levels [29–31].

The kagome lattice is a lattice that can generate a flat band. To date, however, most studies on its flat-band physics have been based on toy models [32–34]. Experimentally, available materials with a kagome lattice are mostly frustrated magnets [35–40], which are half-filled Mott insulators. Unfortunately, the Fermi level (E_F) in such materials is far away from the flat bands. Given the rich bonding chemistry but simple band structure of carbon, e.g., for graphene only p_z states exist near E_F, and the exceptional stabilities of its various allotropes, one may ask if it is possible to synthesize carbon-based kagome or kagome-like lattices and what would be the physics of strong correlation in them.

In this paper, we identify, by first-principles total-energy calculations, a family of two-dimensional (2D) carbon kagome-like structures (to be termed "kagome graphene/graphyne"), which can host flat bands and relevant physical phenomena. The most basic structure is kagome graphene made of carbon triangles on a regular honeycomb lattice. Noticeably, flat bands appear near E_F in all these structures. Upon hole doping, the spin degeneracy of the flat bands

*chenyp@xtu.edu.cn

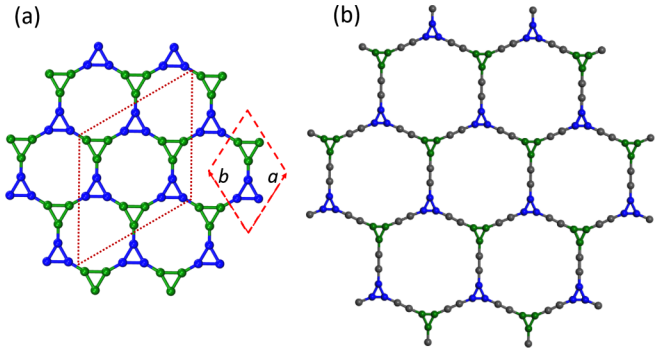

FIG. 1. Atomic structure of (a) kagome graphene, where the primitive unit cell is shown by the dashed red line. Blue and green triangle rings of atoms are two sublattices of the system. Dotted brown line shows a $\sqrt{3} \times \sqrt{3}$ supercell as a result of Wigner crystallization. (b) Kagome graphyne, where the triangular rings are linked by acetylenic carbon linkers.

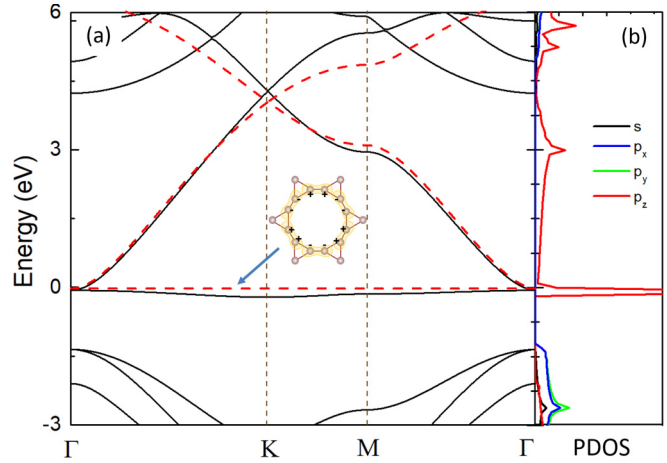

FIG. 2. (a) Band structure of kagome graphene, where the solid and dashed lines are the calculated results of DFT and the tight-binding model in Eq. (1), respectively. Inset shows the wave function for a localized state in the flat band. (b) Partial density of states (PDOS) of kagome graphene.

is spontaneously lifted to result in a flat-band ferromagnetism with a large spin splitting. At a 1/6 filling factor of the flat bands, a Wigner crystallization is found, while at other filling factors various charge-density-wave patterns are expected. These interesting physical phenomena are interpreted based on a Hubbard model. The possibility of realizing an anomalous quantum Hall effect, as well as the possible routes to synthesize kagome graphene, are also discussed.

II. MODEL AND METHODS

The atomic structure of kagome graphene is shown in Fig. 1(a). It has twice as many atoms as a regular kagome lattice, with the two subsets of atoms in Fig. 1(a) denoted by different colors. If the bond length between two adjacent different-colored atoms "shrinks" to zero, one recovers the regular kagome lattice. Other members in the family can be obtained by inserting acetylenic dimers between neighboring triangles. For example, kagome graphyne containing one dimer between triangles is shown in Fig. 1(b). In the following, we focus on kagome graphene, but all the physics discussed below applies equally to other structures as well.

The lattice constant of kagome graphene is $a(=b) = 5.19$ Å. The bond length within a carbon triangle is 1.42 Å, while that between the triangles is 1.35 Å. The former is very close to graphene, while the latter is between graphene and acetylene. Although kagome graphene contains carbon triangles, its cohesive energy of $E_{\text{coh}} = 8.26\,\text{eV/atom}$ is comparable to α- and β-graphynes, 8.28 and 8.35 eV per carbon atom, respectively [41]. To further confirm its lattice stability, we calculated the phonon spectra [see Fig. S1(a) in the Supplementary Information (SI)] [42]. No soft phonon mode is found throughout the Brillouin zone (BZ).

We performed first-principles calculations within the density functional theory (DFT) as implemented in the VASP codes [43]. The potential of the core was described by the projector augmented wave method [44]. The exchange-correlation interaction between the valence electrons was described by the generalized gradient approximation (GGA) using the Perdew-Burke-Ernzerhof (PBE) functional [45]. A kinetic energy cutoff of 600 eV was used. The atomic positions were optimized using the conjugate gradient method, and the energy and force convergence criteria were 10^{-6} eV and 10^{-3} eV/Å, respectively. In the case of kagome graphene, an $11 \times 11 \times 1k$-point mesh was used for the BZ integration.

III. RESULTS AND DISCUSSIONS

A. Band structure

Figure 2(a) shows the band structure of kagome graphene. A flat band appears right below E_F with a bandwidth ~0.1 eV. There are two bands connecting the flat band at the Γ point. They cross each other at the K point, forming a Dirac point but at a considerably higher energy. The flat band is fully occupied while the two Dirac bands are empty. The partial density of states (PDOS) in Fig. 2(b) indicate that these bands can be attributed to out-of-plane carbon p_z orbitals similar to graphene.

The appearance of the almost flat band can be understood by employing a simple tight-binding model. In momentum space, the Hamiltonian reads

$$H_0 = \begin{pmatrix} H_{AA} & H_{AB} \\ H_{BA} & H_{BB} \end{pmatrix}, \tag{1}$$

where H_{AA} and H_{BB} are the intratriangle hopping matrices in sublattice A (red) and B (green) in Fig. 1(a), respectively, and H_{AB} and H_{BA} are the corresponding intertriangle hopping matrices. They are 3×3 matrices of the form

$$\begin{aligned} H_{AA}^{ij} &= H_{BB}^{ij} = t_1(1 - \delta^{ij}), \\ H_{AB}^{ij} &= \left(H_{BA}^{ji}\right)^* = t_2 \delta_{ij} e^{-i\vec{r}_i \cdot k}, \end{aligned} \tag{2}$$

where t_1 and t_2 are the intratriangle and intertriangle hopping amplitudes, respectively, and $\vec{r}_{1,2,3}$ are three vectors from the center of a triangle in the A sublattice to the centers of its three nearest-neighbor triangles in the B sublattice. The tight-binding model with $t_1 = 6\,\text{eV}$ and $t_2 = 3\,\text{eV}$ captures the essential features of the DFT results, as can be seen in

Fig. 2(a). This includes the flat band at $E = t_1 - t_2$, the two Dirac bands with Dirac points at K and K', as well as the quadratic touching between the flat band and the Dirac bands at Γ, which is protected by the group symmetries D_{6h} at Γ and C_{3v} at K (K'). On the other hand, one would not expect the model to work well at higher energies, so we will confine our discussion to states below the Dirac points.

The presence of flat bands in Fig. 2(a) is the result of a special structural property of the kagome graphene lattice, which implies that there exist local single-particle states as the eigenstates of the band Hamiltonian. Consider a real-space state $|a\rangle$, whose charge distribution is within a hexagonal ring as depicted in the inset of Fig. 2(a). We refer to the hexagonal ring as a plaquette in the following text. The state $|a\rangle$ is localized in real space, but it is nevertheless an eigenstate of the Hamiltonian in Eq. (1). This happens because of a total destructive interference of the various hopping amplitudes, which prevents the state from leaking out. The Bloch wave states in the flat band are thus linear combinations of the various $|a\rangle$'s localized in different plaquettes. These localized single-particle states are key to the understanding of strong correlation phenomena.

The flat band and localized states $|a\rangle$ are naturally related to p orbitals on the honeycomb lattice. Consider three linearly independent single-particle states $|1\rangle$, $|2\rangle$, and $|3\rangle$, located on each vertex of a triangle. These states can be decomposed into two irreducible representations (IRREPs) of the lattice symmetry group: the 1D IRREP contains the state $|1\rangle + |2\rangle + |3\rangle$, analogous to the p_z orbital in graphene; the 2D IRREP contains the state $|1\rangle + \omega|2\rangle + \omega^2|3\rangle$ and its time-reversal partner ($\omega = e^{i\,2\pi/3}$), analogous to local $p_x \pm i\,p_y$ orbitals in graphene. The localized states $|a\rangle$'s are the flat-band state, lying fully in the 2D IRREP. In other words, the localized states discussed above are directly mapped to the localized states in the system of p orbitals in the honeycomb lattice [21].

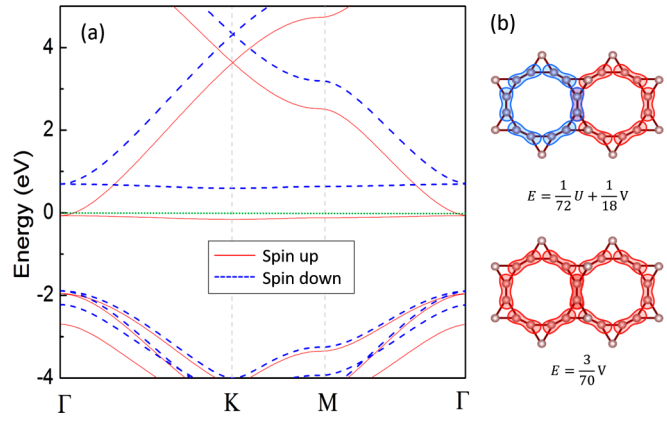

FIG. 3. Flat-band ferromagnetism. (a) DFT band structure of kagome graphene after one-hole doping to result in a ferromagnetic ground state. The green dotted line shows the Fermi level. (b) Wave functions of the localized states in the simplified model [cf. Eq. (1)] with calculated energies. The touching of two localized states with opposite spins would cost more energy than that with the same spin. This energy cost is the origin for the global ferromagnetism seen here.

B. Flat-band ferromagnetism

The interplay between band flatness and Coulomb interaction gives rise to many novel phenomena such as flat-band ferromagnetism [17,18]. Although the Stoner mechanism for ferromagnetism [46] captures the physics of exchange interaction, i.e., spin-polarized electrons maintain a distance from one another due to Fermi statistics to reduce repulsion, it does not take into account the correlation effect. Electrons often remain unpolarized even under very strong interactions since they can still avoid one another by developing highly correlated wave functions [47]. Spin polarization is typically not favored because the kinetic energy cost is often larger than the exchange energy gain. This competition imposes a serious challenge to obtain itinerant ferromagnetism. In contrast, when electrons fill in the flat band, the kinetic energy penalty of spin polarization does not exist anymore, hence the exchange interaction stabilizes the polarized state. To obtain some insights from DFT calculations, we dope the system by reducing the density of valence electrons (hole doping) to make the flat band partially filled, say $\nu = \frac{1}{2}$, while maintaining the charge neutrality with a compensating homogeneous background charge. In experiments, doping can be achieved by an electrostatic gating. Figure 3(a) shows the band structure of the doped ferromagnetic ground state, which is spontaneously spin-polarized. The spin-up and -down bands split, with E_F straddling between the upper empty and lower occupied flat bands. The spin splitting is $\Delta E = 768$ meV, which is roughly on the order of the on-site Coulomb interaction. The cohesive energy of the ferromagnetic ground state is 8.24 eV/atom, which is about 20 meV/atom larger than the nonpolarized state. The lattice constant is increased slightly to 5.27 Å, while all the bond lengths are changed to 1.41 Å. Figure S1(b) of the SI shows the phonon spectrum for the hole-doped kagome graphene, showing that the structure is stable.

C. Wigner crystallization due to the flat band

When the filling inside the flat band is less than $\nu = \frac{1}{2}$, Coulomb interaction can further organize the electrons in the flat band, leading to other interesting phenomena. For instance, Wigner crystallization occurs at $\nu = \frac{1}{6}$, which spontaneously breaks the original translational symmetry of the crystal [21]. A new translational symmetry should emerge, but one that is entirely driven by the electron degree of freedom, namely a Wigner crystallization. A simple analysis shows that a $\sqrt{3} \times \sqrt{3}$ supercell [as marked by the dotted brown lines in Fig. 1(a)], which is rotated 30° from the original cell, is consistent with such a filling of the flat band. Due to the effect of band folding, the original spin-up flat band splits into three bands [see Fig. 4(a)], only one of which is fully occupied to result in a charge gap $\Delta_c \sim 90$ meV with the other two completely empty bands. The lattice constant is also increased from 8.99 to 9.53 Å. Figure 4(b) shows the charge density of the occupied flat-band state, revealing that only $\frac{1}{3}$ of the plaquettes are now occupied. Figure 4(c) shows the magnetic moments on atoms. One can see that this Wigner crystal is ferromagnetic with a moment of $0.055\mu_B$ for atoms on the closed loops inside the occupied plaquettes and $-0.021\mu_B$ for atoms connecting the loops.

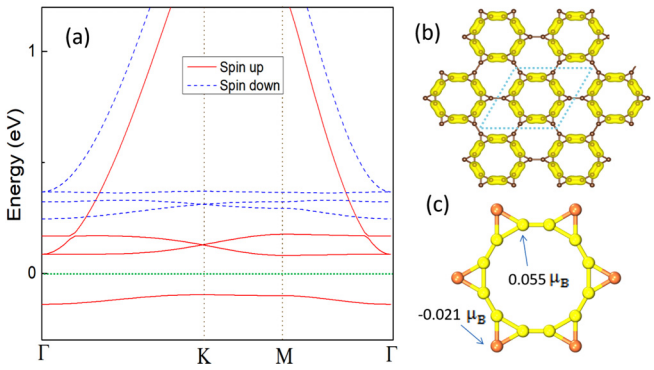

FIG. 4. (a) Band structure of kagome graphene in the $\sqrt{3} \times \sqrt{3}$ supercell doped by five holes, i.e., the filling factor is $1/6$ for the flat band. The green dotted line shows the Fermi level. (b) Charge-density contour for states (at any k-point) in the occupied flat band in panel (a). It leads to a Wigner crystallization, whose unit cell is shown in the light-blue dotted diamond. Each yellow electron ring corresponds to a single electron. (c) Magnetic moments of carbon atoms in the supercell.

It should be noted that, in the conventional setting, Wigner crystallization is a strongly correlated phenomenon resulting from the competition between kinetic energy and interaction energy. The DFT calculation, due to its improper treatment of the electron self-interactions, tends to produce the so-called delocalization error, which is always in favor of delocalized states, hence there is a general lack of Wigner crystallization. However, here we have a flat band arising from the special kagome lattice configuration for which the kinetic energy is completely quenched such that the interaction term always wins. In other words, the actual wave-function localization, and hence the formation of the Wigner lattice, due to Coulomb repulsion, can only be more pronounced than what we can obtain using the DFT approach. This will be validated qualitatively by the following mean-field-theory analysis.

D. Explanation in terms of the Hubbard model

To understand the above results, we employ the following model of interacting electrons to describe the kagome-graphene structure:

$$H = H_0 + U \sum_i n_{i,\uparrow} n_{i,\downarrow} + V \sum_{\langle i,j \rangle} (n_{i,\uparrow} + n_{i,\downarrow})(n_{j,\uparrow} + n_{j,\downarrow}), \tag{3}$$

where H_0 is the noninteracting tight-binding Hamiltonian introduced in Eq. (1); U and V describe the on-site and nearest-neighboring Coulomb repulsions, respectively. As we will demonstrate below, this minimal model captures the essential physics of both flat-band ferromagnetism and Wigner crystallization.

We first discuss the ferromagnetism occurring at $\nu = \frac{1}{2}$. At this filling, each of the localized states $|a\rangle$ in different plaquettes is occupied by one electron. If no electron-electron interaction is included, the spin direction of each localized plaquette state is arbitrary, leading to massive degenerate ground states. Because the localized states of neighboring plaquettes overlap on the bonds they share, the direct exchange interaction dominates, which arises from the two-electron exchange integrals of the on-site and nearest-neighboring repulsions, and it favors that the two neighboring localized states have the same spin direction. As a consequence, the fully polarized spin configuration is selected as the ground state, exhibiting flat-band ferromagnetism. The key here is that the kinetic energy is quenched in the flat band while the interaction effect is amplified. In Fig. S2(a) of the SI, we show the mean-field calculation of the band structure with $U = 2.8\,\text{eV}$ and $V = 1\,\text{eV}$, which agrees well with the DFT results.

The ferromagnetism persists at lower fillings. To understand this, consider the process of filling electrons in the flat band. At low filling, electrons can avoid each other by occupying the localized states centered at plaquettes disconnected with each other, and the interaction energy is simply zero if only the onsite and nearest-neighboring repulsions are taken into account. Each localized state is free to choose between spin-up or -down. As the filling increases, more plaquette localized states are occupied. Beyond $\nu = \frac{1}{6}$, no more plaquette localized states are available to fill; the occupied flat-band states have to touch each other, so their interactions start to have an effect. The touching between two neighboring plaquettes of opposite spins costs an energy of $\frac{1}{72} U + \frac{4}{315} V$ compared with that of the same spin [see Fig. 3(b)]. Consequently, domains constituted by connected plaquette localized states are polarized, and their length scale increases with ν. As the filling reaches the percolation threshold $\nu = \frac{1}{4}$ [48], the area of the largest connected domains scales with the system area, hence the global magnetization M is developed, which peaks at $\nu = \frac{1}{2}$.

Now we consider the Wigner crystallization at $\nu = \frac{1}{6}$. This particular filling corresponds to the closest packing configuration of occupied plaquette localized states without touching each other, as depicted in Fig. 4(b). This is an incompressible phase, as any change of the closest packing configuration would result in an energy increase due to the nearest-neighbor repulsion between plaquettes. It spontaneously breaks the original lattice translational symmetry to result in an enlarged $\sqrt{3} \times \sqrt{3}R30^\circ$ supercell. This symmetry breaking is consistent with the DFT results in Fig. 4(a). As a matter of fact, the standard mean-field treatment of Eq. (3) also reproduces quantitatively the DFT band structure, as can be seen in Fig. S2(b) in the SI. As discussed earlier, if only the on-site and nearest-neighboring interaction are considered as in the minimal model, the Wigner crystal at $\nu = \frac{1}{6}$ should be paramagnetic as each plaquette can pick a random spin direction without affecting the total energy. However, the realistic system studied by DFT includes hoppings beyond nearest neighbors. In this case, the plaquette wave functions are no longer exactly localized, but slightly extend outside as evidenced by the small dispersion of the band in Fig. 4(a), such that different plaquette wave functions overlap to generate exchange interaction in favor of ferromagnetism.

Note that the DFT calculation and the discussion above are limited to $\nu = \frac{1}{6}$. As Coulomb interaction is a long-range interaction, one can expect that at lower than $\frac{1}{6}$ fillings, Wigner crystals of different patterns should also be stabilized [49].

Next, we would like to briefly mention the possibility of realizing the anomalous quantum Hall effect in kagome

graphene, whose band structure shows quadratic touches of the flat band with Dirac bands. In general, a quadratic-touching point is unstable in the presence of even an infinitesimal interaction [50], which lifts the degeneracy by opening a gap. In our case at $\nu = \frac{1}{2}$, the spin-polarized flat band spontaneously breaks the time-reversal symmetry in the orbital channel to open a gap. In each triangle, therefore, there is a spontaneously developed nonzero orbital angular momentum L_z around the center of the plaquette, as an order parameter. Consequently, the originally flat band develops a dispersion near the Γ point, and acquires a nontrivial topological Chern number 1 or -1. The Chern number is obtained by numerically integrating the Berry curvature $i\partial_{k_x}\langle\psi(\vec{k})|\partial_{k_y}|\psi(\vec{k})\rangle - i\partial_{k_y}\langle\psi(\vec{k})|\partial_{k_x}|\psi(\vec{k})\rangle$ over the discretized Brillouin zone [51], where $|\psi(\vec{k})\rangle$ is the Bloch state obtained from the mean-field theory. Using Eq. (3) with the same parameters as before, we obtain $L_z = 0.004\hbar$. Figures S3(a) and S3(b) in the SI show that a gap of $\sim$5 meV opens up between the flat and Dirac bands, which corresponds to a temperature of about 60 K. Hence, at a reasonably low temperature, chiral edge modes should be observed in a kagome graphene ribbon [see Figs. S3(c) and S3(d)].

E. Experimental feasibility of kagome graphene

To fabricate the kinetically stable kagome graphene, one may consider the following (as detailed in Fig. S4): the bottom line is that the elemental building unit of the triangular carbon rings of kagome graphene already exists in the laboratory as various cyclopropane molecules. One may thus tailor the ligand chemistry of the cyclopropanes to realize a self-assembly of the kagome graphene, similar to the recent success in self-assembling metastable carbon nanowiggles. In terms of the choice of substrate, the self-assembly process may be carried out on a single-layer boron nitride sheet. According to our calculation, the mismatch between a 2×2 supercell of boron nitride and the primitive cell of kagome graphene is smaller than 2.1%. The binding energy between kagome graphene and boron nitride is comparable to that of graphene on the same substrate. For more details, see Fig. S4 in the SI, which also shows that the flat band and related phenomena are intact.

F. Other related carbon structures

We would like to point out that the aforementioned flat-band physics applies not only to kagome graphene, but also to a whole family of related structures, for example the one in Fig. 1(b) where the triangular rings are linked by acetylenic dimers. We will term such a structure kagome graphyne. Here, the lattice constant is $a' = b' = 9.65$ Å, the bond length within the triangular ring is 1.42 Å, that within the acetylenic linker is 1.25 Å, and that between the ring and linker is 1.34 Å. The phonon spectrum in Fig. S1(c) in the SI indicates that kagome graphyne is also kinetically stable, although its cohesive energy of $E_{\rm coh} = 8.19$ eV/atom is lower than that of kagome graphene, due to the less-stable acetylenic bonds. Figure S5(b) shows that the band structure of kagome graphyne, with an almost dispersionless flat band right above E_F, can be even better than that of kagome graphene. As a result, spontaneous spin polarization and Wigner crystallization after hole doping are also obtained. When the triangular rings are connected by more acetylenic dimers, a series of carbon structures similar to kagome graphene, such as a kagome graphdiyne, will be obtained. Besides pure carbon networks, covalent organic frameworks such as COF-1 may also be viewed as having a local kagome structure.

IV. CONCLUSION

We show by first-principles calculations that kagome graphene and related structures are promising artificial materials to study the physics of strong correlation, while traditional carbon-based materials are not. The key is the unusual kagome structure of carbon atoms, all of which exhibit a flat band right below E_F. A tight-binding model is constructed to explain these findings by localized single-particle states as a result of destructive interference among various electron hopping processes. The interplay between band flatness and electron coupling leads to a number of interesting properties, such as ferromagnetism, Wigner crystallization, and the anomalous quantum Hall effect. Last but not least, we also propose potential synthesis pathways to fabricate kagome graphene and related structures.

Recently, Cao *et al.* reported that a bilayer magic-angle graphene superlattice exhibits ultraflat bands near charge neutrality due to the strong interlayer coupling [52,53]. These flat bands exhibit correlated insulating phases at half-filling, which are not expected in a noninteracting picture. Upon electrostatic doping away from these correlated insulating states, tunable zero-resistance states are observed. These results are complementary with ours, which jointly open a door to explore exotic many-body quantum phases in 2D carbon materials without an external magnetic field.

ACKNOWLEDGMENTS

Work in China was supported by the National Natural Science Foundation of China (No. 51376005, No. 11474243, and No. 11729402), work at RPI was supported by US DOE under Grant No. DE-SC0002623, and work at UCSD was supported by NSF DMR-14103751.

[1] H. W. Kroto, J. R. Heath, S. C. O'Brien, R. F. Curl, and R. E. Smalley, Nature (London) **318**, 162 (1985).
[2] S. Iijima, Nature (London) **354**, 56 (1991).
[3] K. S. Novoselov, A. K. Geim, S. V. Morozov, D. Jiang, Y. Zhang, S. V. Dubonos, I. V. Grigorieva, and A. A. Firsov, Science **306**, 666 (2004).
[4] K. S. Novoselov and A. Geim, Nat. Mater. **6**, 183 (2007).
[5] Y. Zhang and Y. Tan, Nature (London) **438**, 201 (2005).
[6] C. Neto, Rev. Mod. Phys. **81**, 109 (2009).
[7] S. Ghosh, W. Bao, D. L. Nika, S. Subrina, E. P. Pokatilov, C. N. Lau, and A. A. Balandin, Nat. Mater. **9**, 555 (2010).

[8] C. Lee, X. Wei, J. W. Kysar, and J. Hone, Science **321**, 385 (2008).

[9] A. A. Balandin, S. Ghosh, W. Bao, I. Calizo, D. Teweldebrhan, F. Miao, and C. N. Lau, Nano. Lett. **8**, 902 (2008).

[10] Y. Xie, Y. Chen, X. L. Wei, and J. Zhong, Phys. Rev. B **86**, 195426 (2012).

[11] Y. Li, W. Zhou, H. Wang, L. Xie, Y. Liang, F. Wei, J.-C. Idrobo, S. J. Pennycook, and H. Dai, Nat. Nanotechnol. **7**, 394 (2012).

[12] Y. P. Chen, Y. E. Xie, L. Sun, and J. Zhong, Appl. Phys. Lett. **93**, 092104 (2008).

[13] R. Raccichini, A. Varzi, S. Passerini, and B. Scrosati, Nat. Mater. **14**, 271 (2015).

[14] Y. Chen, Y. Xie, S. A. Yang, H. Pan, F. Zhang, M. L. Cohen, and S. Zhang, Nano. Lett. **15**, 6974 (2015).

[15] Q. H. Wang and M. C. Hersam, Nat. Chem. **1**, 206 (2009).

[16] S. Bae *et al.*, Nat. Nanotechnol. **5**, 574 (2010).

[17] H. Tasaki, Phys. Rev. Lett. **69**, 1608 (1992).

[18] A. Mielke, J. Phys. A **24**, L73 (1991).

[19] E. Wigner, Phys. Rev. **46**, 1002 (1934).

[20] F. Pollmann, P. Fulde, and K. Shtengel, Phys. Rev. Lett. **100**, 136404 (2008).

[21] C. Wu, D. Bergman, L. Balents, and S. Das Sarma, Phys. Rev. Lett. **99**, 070401 (2007).

[22] C. Wu and S. Das Sarma, Phys. Rev. B **77**, 235107 (2008).

[23] T. Jacqmin, I. Carusotto, I. Sagnes, M. Abbarchi, D. D. Solnyshkov, G. Malpuech, E. Galopin, A. Lemaître, J. Bloch, and A. Amo, Phys. Rev. Lett. **112**, 116402 (2014).

[24] K. Noda, K. Inaba, and M. Yamashita, Phys. Rev. A **90**, 043624 (2014).

[25] R. A. Vicencio, C. Cantillano, L. Morales-Inostroza, B. Real, C. Mejía-Cortés, S. Weimann, A. Szameit, and M. I. Molina, Phys. Rev. Lett. **114**, 245503 (2015).

[26] S. Mukherjee, A. Spracklen, D. Choudhury, N. Goldman, P. Öhberg, E. Andersson, and R. R. Thomson, Phys. Rev. Lett. **114**, 245504 (2015).

[27] B. Jaworowski, A. D. Güçlü, P. Kaczmarkiewicz, M. Kupczyński, P. Potasz, and A. Wójs, New J. Phys. **20**, 063023 (2018).

[28] G. Volovik, J. Supercond. Nov. Magn. **26**, 2887 (2013).

[29] E. Tang, J.-W. Mei, and X.-G. Wen, Phys. Rev. Lett. **106**, 236802 (2011).

[30] K. Sun, Z. Gu, H. Katsura, and S. Das Sarma, Phys. Rev. Lett. **106**, 236803 (2011).

[31] T. Neupert, L. Santos, C. Chamon, and C. Mudry, Phys. Rev. Lett. **106**, 236804 (2011).

[32] C. Rüegg, Nat. Phys. **6**, 837 (2010).

[33] G.-B. Jo, J. Guzman, C. K. Thomas, P. Hosur, A. Vishwanath, and D. M. Stamper-Kurn, Phys. Rev. Lett. **108**, 045305 (2012).

[34] E. Goremychkin, R. Osborn, B. Rainford, R. Macaluso, D. Adroja, and M. Koza, Nat. Phys. **4**, 766 (2008).

[35] K. Matan, T. Ono, Y. Fukumoto, T. Sato, J. Yamaura, M. Yano, K. Morita, and H. Tanaka, Nat. Phys. **6**, 865 (2010).

[36] S. V. Isakov, R. G. Melko, and M. B. Hastings, Science **335**, 193 (2012).

[37] C. Castelnovo, R. Moessner, and S. L. Sondhi, Nature (London) **451**, 42 (2008).

[38] P. W. Anderson, Science **235**, 1196 (1987).

[39] C. Nisoli, R. Moessner, and P. Schiffer, Rev. Mod. Phys. **85**, 1473 (2013).

[40] L. Balents, Nature (London) **464**, 199 (2010).

[41] N. Narita, S. Nagai, S. Suzuki, and K. Nakao, Phys. Rev. B **58**, 11009 (1998).

[42] See Supplemental Material at http://link.aps.org/supplemental/10.1103/PhysRevB.98.035135 for phonon spectra of Kagome structures, band structures calculated by mean field theory, possible ways of a Kagome graphene on top of a boron nitride substrate, and DFT band structure of a Kagome graphyne.

[43] G. Kresse and J. Hafner, Comput. Mater. Sci. **6**, 15 (1996).

[44] G. Kresse and D. Joubert, Phys. Rev. B **59**, 1758 (1999).

[45] J. P. Perdew, K. Burke, and M. Ernzerhof, Phys. Rev. Lett. **77**, 3865 (1996).

[46] E. C. Stoner, Proc. R. Soc. London, Ser. A **165**, 372 (1938).

[47] E. Lieb and D. Mattis, Phys. Rev. **125**, 164 (1962).

[48] S. Zhang, H.-h. Hung, and C. Wu, Phys. Rev. A **82**, 053618 (2010).

[49] M. Modarresi and A. D. Güçlü, Phys. Rev. B **95**, 235103 (2017).

[50] K. Sun, H. Yao, E. Fradkin, and S. A. Kivelson, Phys. Rev. Lett. **103**, 046811 (2009).

[51] T. Fukui, Y. Hatsugai, and H. Suzuki, J. Phys. Soc. Jpn. **74**, 1674 (2005).

[52] Y. Cao *et al.*, Nature (London) **556**, 43 (2018).

[53] Y. Cao *et al.*, Nature (London) **556**, 80 (2018).